

# A dynamically extending exclusion process

**K. E. P. Sugden and M. R. Evans**

SUPA, School of Physics, University of Edinburgh,  
Mayfield Road, Edinburgh EH9 3JZ, UK.

E-mail: [k.e.p.sugden@sms.ed.ac.uk](mailto:k.e.p.sugden@sms.ed.ac.uk), [m.evans@ed.ac.uk](mailto:m.evans@ed.ac.uk)

**Abstract.** An extension of the totally asymmetric exclusion process, which incorporates a dynamically extending lattice is explored. Although originally inspired as a model for filamentous fungal growth, here the dynamically extending exclusion process (DEEP) is studied in its own right, as a nontrivial addition to the class of nonequilibrium exclusion process models. Here we discuss various mean-field approximation schemes and elucidate the steady state behaviour of the model and its associated phase diagram. Of particular note is that the dynamics of the extending lattice leads to a new region in the phase diagram in which a shock discontinuity in the density travels forward with a velocity that is lower than the velocity of the tip of the lattice. Thus in this region the shock recedes from both boundaries.

PACS numbers: 05.60.-k, 87.16.Ac, 05.70.Ln, 87.10.+e

## 1. Introduction

When studying the physics of systems from the natural world, it is not surprising that one finds many problems which lie outside the realm of equilibrium physics. Rather, we are more likely to find systems which reach some sort of nonequilibrium steady state, characterised by non zero energy flow or other currents. For studying such systems, a vibrant collection of models has emerged. Many of the models have been studied extensively, not only for their applications but also for their intrinsically interesting behaviour [1].

The asymmetric simple exclusion process (ASEP) is a paradigmatic model for simple nonequilibrium driven diffusive systems [2]. It comprises a one dimensional lattice along which hard-core particles hop, with some bias in direction. Despite its simplicity, this model is capable of showing a range of interesting phenomena including boundary induced phase transitions, shock formation and spontaneous symmetry breaking. Over the years the application of the ASEP has been wide and varied, but it particularly lends itself to the modelling of transport problems [3], for example the motion of molecular motors along microtubule filaments in biophysical systems [4, 5, 6, 7]. Indeed the ASEP was originally introduced as a lattice model of ribosome motion along mRNA [8].

Recently, a particular case of the ASEP; the totally asymmetric exclusion process (TASEP), was generalised to incorporate a dynamically extending lattice [9, 10]. The new variation allows a particle reaching the end of a lattice to extend it by converting into a single new site. In this way, a connection is made between the microscopic constituents of the model and the dynamics of the system size. We also note that very recently an asymmetric exclusion process with Langmuir kinetics and a dynamic boundary has also been studied [11].

The model of [9, 10] was motivated by a problem in mycology: the process of filamentous fungal growth, where continuous growth of the filament tip is maintained by a supply of mass transported from behind the tip to the site of growth. In [9] it was argued that one could model the transport of vesicles by molecular motors along the network of microtubule fragments by an ensemble of continuous effective microtubules acting as dynamically extending asymmetric exclusion processes. Preliminary mean-field and simulation results showed that various growth regimes occurred, in particular regimes exhibiting a high density of motors near the tip.

In this work, the extending TASEP of [9] is discussed in its own right, as a nontrivial addition to the existing class of exclusion process models. We discuss how steady states may arise in this growing system, and extend the well established TASEP phase diagram into a 3-dimensional parameter space. As with the TASEP, we may derive the phase diagram through a phenomenological approach which considers the dynamics of a *shock* that travels between the boundaries of the lattice. Through this approach, we arrive at a new subregion in the phase diagram in which a shock is moving away from both boundaries and thus persists in the system. We develop a series of mean-field approximations for our analysis.

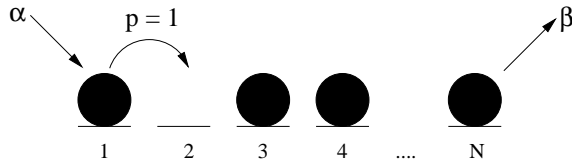


**Figure 1.** Schematic of the open boundary TASEP with input rate  $\alpha$ , hop rate  $p = 1$  and extraction rate  $\beta$ .

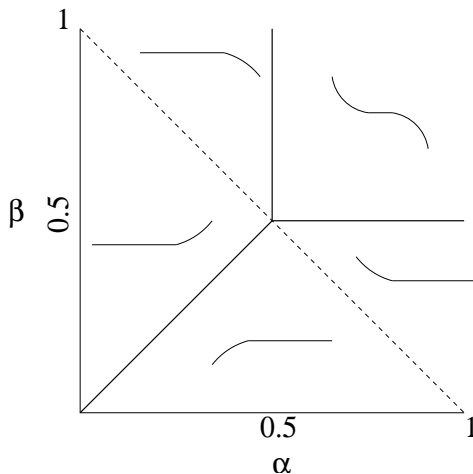


**Figure 2.** The phase diagram for the TASEP with schematic density profiles. Three distinct phases exist. For  $\alpha$  or  $\beta < 0.5$ , two phases are possible; a high density phase for  $\alpha > \beta$  and a low density phase for  $\beta > \alpha$ . When  $\alpha$  and  $\beta > 0.5$ , the system is in a phase of maximum current, no longer limited by the input or output rate.

The simplest scheme, which for the ASEP actually predicts the correct phase diagram [12], only predicts the phases qualitatively. However a refined mean-field approximation predicts phase boundaries which are rather close to those we determine by Monte Carlo simulations. A heuristic argument which considers the symmetry between particles entering one end of the lattice and ‘holes’ entering the opposite end provides a further prediction for the phase diagram which is very close indeed to that predicted by the refined mean-field theory. We find that this prediction is in fact the best fit to the simulation data.

The paper is organised as follows: In section 2, we review the TASEP and introduce the dynamically extending model. In section 3 the model is formally defined and in section 4 a simple mean-field approximation is used to analytically approximate the steady states. In section 5 the mean-field approximation is extended to include correlations between sites 1 and 2, resulting in a refined prediction of the model’s phase boundaries. In section 6, we discuss the heuristic argument and the resulting phase diagram which appears to be in closest agreement with simulation. The Monte Carlo simulation results are discussed in section 7, where phase diagrams for the model are also presented. Finally, we conclude in section 8.

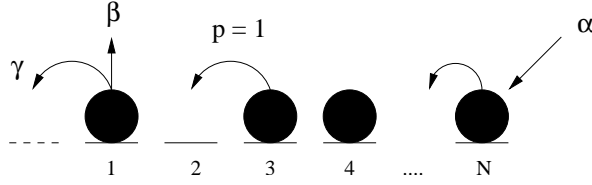


**Figure 3.** Schematic of the model with input rate  $\alpha$ , hop rate  $p = 1$ , desorption rate  $\beta$  and growth rate  $\gamma$ .

## 2. A TASEP based model

We begin by reviewing the well-known TASEP, upon which the dynamically extending exclusion process we study is based. It comprises particles that hop along a one-dimensional lattice in a single direction. No more than one particle may occupy each lattice site at any given time. Particles are injected at one end of the lattice and removed from the other end with rates  $\alpha$  and  $\beta$ , which are the only control parameters for the model. In the bulk of the lattice, the hops occur with rate 1. Figure 1 illustrates the TASEP schematically.

The behaviour of this system is categorised in terms of its *steady state phases*. A steady state is reached when the density of each site, that is the time-averaged occupancy, no longer changes with time. Equivalently, when the system is in a steady state, the current of particles along the lattice is the same everywhere. The phases are defined by the system's macroscopic properties in the large system limit i.e. the particle density *profile* across the lattice and the particle current between any two neighbouring lattice sites. Phase transitions are induced by varying the boundary conditions, controlled by parameters  $\alpha$  and  $\beta$ . The exact phase behaviour of the TASEP is well understood from the exact solution [13, 14] as well as mean-field [12] and other approaches [2]. Three distinct steady state phases exist. For low input,  $\alpha < 0.5$ , and  $\alpha < \beta$ , the system is in a low density phase, where the bulk of the lattice is at a low density equal to  $\alpha$  and the current is equal to  $\alpha(1 - \alpha)$ . When at  $\alpha = \beta$ , there is a discontinuous phase transition and the system enters a high density phase, now limited by a low output rate  $\beta < 0.5$ . The bulk of the lattice in this phase is at a high density equal to  $1 - \beta$  and the current is equal to  $\beta(1 - \beta)$ . When  $\alpha$  and  $\beta$  are both  $> 0.5$ , the system enters a phase of maximal current. The system is no longer controlled by the input and output rates, instead the bulk density is  $1/2$  and the current is  $1/4$ . Furthermore, the density profile decays algebraically from the boundaries towards the bulk value  $1/2$ . The results are summarised in the phase diagram of Figure 2.

The model discussed in the following work has an additional third parameter,  $\gamma$ , which is the rate at which a particle reaching the ultimate lattice site may convert into a new lattice site, thus extending the length of the lattice by 1. We shall explore the resultant phase structure in the three dimensional parameter space of  $\alpha$ ,  $\beta$  and  $\gamma$ .

### 3. The DEEP

The dynamically extending exclusion process (DEEP) is defined by the rates at which the following processes occur: particles in the bulk hop to the left with rate 1; particles enter the lattice from the right with rate  $\alpha$ ; at site 1 two processes may occur, particles detach from site 1 with rate  $\beta$  and particles may transform into a new lattice site with rate  $\gamma$ . These processes are illustrated schematically in Figure 3. Thus  $\gamma$  is the parameter controlling the lattice growth,  $\beta$  allows particles to leave the end of the lattice without extending it and ratio  $\gamma/\beta$  controls the efficiency with which the lattice extends.

Indicating the presence of a particle by 1 and an empty lattice site by 0 the stochastic dynamics is

$$01 \rightarrow 10 \quad \text{with rate } 1, \quad (1)$$

$$\text{at site 1} \quad 1 \rightarrow 0 \quad \text{with rate } \beta \quad (2)$$

$$\text{at site 1} \quad 1 \rightarrow 00 \quad \text{with rate } \gamma, \quad (3)$$

$$\text{at the rightmost site} \quad 0 \rightarrow 1 \quad \text{with rate } \alpha. \quad (4)$$

Note the direction of particle hopping is to the *left* (as opposed to most studies of the TASEP where the direction is to the right) for reasons which will soon become apparent. This choice is of course immaterial.

Also note that under the simultaneous reversal of the direction of particle hopping and interchange of  $\alpha$  and  $\beta$ , the TASEP enjoys an exact particle-hole symmetry at the microscopic level, while the DEEP does not. This is due to ‘growth’ rule 3, which has no counterpart at the right boundary.

#### 3.1. Exact steady state equations

In the DEEP model the system size is not conserved and continually increases, therefore care must be taken to define what is meant by a steady state. For example, the density at site  $i$  will generally only become stationary with respect to a particular frame of reference. Two natural frames to consider are the frame moving with the tip, in which case the tip is always at site 1 and the site label  $i$  measures the distance from tip, and the stationary frame where the right boundary is always at site 1 and the tip is at site  $N$  where  $N$  increases as the lattice extends. A phase of the system is specified by stationary values of the densities and the frame of reference. Moreover we shall encounter one phase, the maximal current phase, that does not satisfy this criterion and instead is only quasi-stationary.

To begin with, we choose to work in the reference frame of the growing lattice tip, so that the leftmost site is always labelled site 1. The input end of the lattice is site  $N(t)$  and process (4) may be formulated as there being a reservoir of particles of density  $\alpha$  at site  $N(t) + 1$ . As time  $t \rightarrow \infty$  the system size  $N(t) \rightarrow \infty$ , therefore we may write a boundary

condition at the input end of the lattice as

$$\alpha = \lim_{N \rightarrow \infty} \langle \tau_N \rangle . \quad (5)$$

We now construct the equations for the steady state dynamics. Note that when a growth event occurs, via process (3), all the previous lattice sites are relabelled  $i \rightarrow i + 1$ . The exact equations for correlations functions in the steady state are:

$$\frac{d\langle \tau_1 \rangle}{dt} = 0 = \langle [1 - \tau_1] \tau_2 \rangle - (\gamma + \beta) \langle \tau_1 \rangle , \quad (6)$$

$$\frac{d\langle \tau_2 \rangle}{dt} = 0 = \langle [1 - \tau_2] \tau_3 \rangle - \langle [1 - \tau_1] \tau_2 \rangle - \gamma \langle \tau_1 \tau_2 \rangle , \quad (7)$$

$$\frac{d\langle \tau_i \rangle}{dt} = 0 = \langle [1 - \tau_i] \tau_{i+1} \rangle - \langle [1 - \tau_{i-1}] \tau_i \rangle + \gamma \langle \tau_1 [\tau_{i-1} - \tau_i] \rangle \quad i \geq 3 . \quad (8)$$

Where  $\tau_i$  is the occupancy at site  $i$  and can take on a value 1 or 0. The angle brackets denote an average in the steady state. Thus  $\langle \tau_i \rangle$  is the average occupancy in the steady state or particle *density* at site  $i$ . These equations may be understood in terms of a particle *current* along the lattice. The positive terms represent the current of particles entering the site from the right and the negative terms represent the current leaving to the left. The dynamics at sites 1 and 2 differ from those of the rest of the system due to the transition from particle to lattice site. In the steady state, the current ‘in’ balances the current ‘out’ everywhere. We thus obtain from (6-8) the following exact expressions for the conserved steady state particle current  $J$ :

$$J = (\gamma + \beta) \langle \tau_1 \rangle , \quad (9)$$

$$J = \langle \tau_2 [1 - \tau_1] \rangle , \quad (10)$$

$$J = \langle \tau_{i+1} [1 - \tau_i] \rangle - \gamma \langle \tau_1 \tau_i \rangle \quad i \geq 2 . \quad (11)$$

The rate of lattice extension, or tip velocity, is given by:

$$v = \gamma \langle \tau_1 \rangle , \quad (12)$$

which leads us to a relation between the current and velocity:

$$J = v \left( 1 + \frac{\beta}{\gamma} \right) . \quad (13)$$

Our approach to solve the system of equations (9–11) is to take a mean field approximation in order to analyse the steady state equations and determine the phases and phase boundaries of the system.

#### 4. Simple mean-field theory

In the simplest mean field approximation, we replace

$$\langle \tau_i \tau_j \rangle = \rho_i \rho_j \quad \forall i, j \ (i \neq j) \quad (14)$$

where  $\rho_i = \langle \tau_i \rangle$  is the average steady state density at site  $i$ , and we ignore correlations between the density at different sites [12]. Equation (11) then gives the recurrence relation:

$$\rho_{i+1} = \frac{J + v\rho_i}{1 - \rho_i} \quad i \geq 2. \quad (15)$$

We find  $\rho_1, \rho_2$  from (9), (10) and (13):

$$\rho_1 = \frac{J}{\gamma + \beta} \quad (16)$$

$$\rho_2 = \frac{J}{1 - \rho_1} = \frac{J(\gamma + \beta)}{\gamma + \beta - J}. \quad (17)$$

The recurrence (15) together with the initial condition (17) determine all  $\rho_i$  in terms of  $J$  (or  $v$ ). It remains to fix  $J$  self-consistently to determine the various phases.

*Low density Phase:* The recurrence (15) has two fixed points

$$\rho_{\pm} = \frac{1 - v \pm \sqrt{(1 - v)^2 - 4J}}{2}. \quad (18)$$

The lower of the fixed points is stable, so for  $\rho_2$  within the basin of attraction, the density iterates to this value and the density profile converges rapidly to a constant density in the bulk of the lattice. See Figure 4 for a graphical representation of the iterative solutions to (15). To meet boundary condition (5), we define the lower fixed point:

$$\rho_- = \alpha. \quad (19)$$

It follows from (18) that the upper fixed point is then:

$$\rho_+ = 1 - v - \alpha. \quad (20)$$

The boundary condition (5) fixes  $v$  using (13) and (15):

$$v_{ld} = \frac{\alpha(1 - \alpha)}{1 + \alpha + \frac{\beta}{\gamma}}, \quad (21)$$

and the corresponding current is  $J_{ld} = (1 + \beta/\gamma)v_{ld}$ .

The condition for this phase is that  $\rho_2 < \rho_+$  so that  $\rho_i \rightarrow \rho_-$  as  $i \rightarrow \infty$ . Using (20) and (21) this condition reduces to

$$\gamma > \frac{\alpha - \beta}{1 + \alpha}. \quad (22)$$

This is the phase boundary for the low density phase.

The density in the bulk of the low density phase is limited by a low input rate  $\alpha$ . At the tip there is a decay to the boundary condition (19) determined by rates  $\beta$  and  $\gamma$ . The low density region is split into two subregions distinguished by whether the tip density is above or below  $\alpha$ . For  $\rho_2 < \alpha$ , the tip density is less than  $\alpha$  and for  $\alpha < \rho_2 < 1 - v - \alpha$ , the tip density is greater than  $\alpha$ .

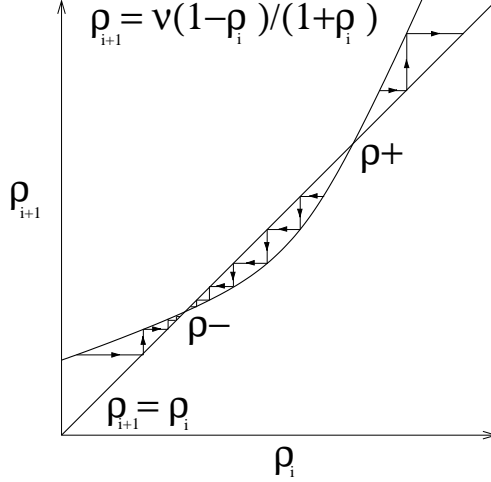


**Figure 4.** A graphical representation of the solutions to the recurrence relation (15). Iterations beginning below the unstable upper fixed point,  $\rho_+$ , converge to the stable lower fixed point,  $\rho_-$ .

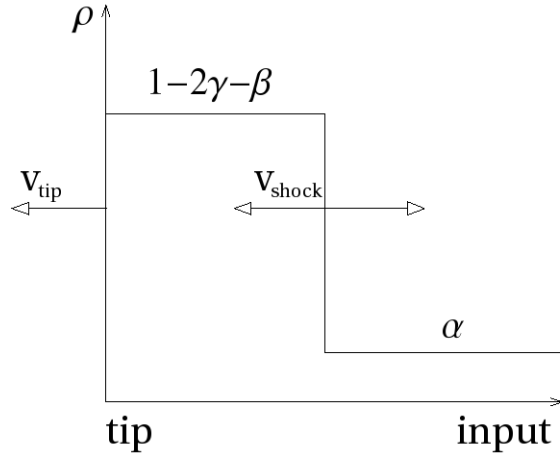


**Figure 5.** A shock is set up between regions in the lattice with a high density (next to the tip) and low density (far from the tip). The shock travels with a velocity fixed through mass conservation, which may be different to the velocity of the lattice tip.

*High density phase:* Another possible solution to (15) and (5) is that  $\rho_2 = \rho_+$ . In this case the recurrence (15) yields  $\rho_i = \rho_+$  for  $i \geq 2$ . The phenomenological interpretation is that when  $\gamma$ , the rate of release of particles at the growing end, is no longer large enough to control the input rate; the particle density near the tip reaches a maximum value  $\rho_+$  that extends back through the lattice. The high density in the bulk  $\rho_+$  is then connected to the density at the input boundary  $\alpha$ , with a discontinuous *shock*. Mass conservation implies a



speed for the shock,  $v_s$ , given by:

$$v_s = 1 - \rho_+ - \alpha . \quad (23)$$

The shock solution is illustrated schematically in Figure 5.

Defining  $\rho_2 = \rho_+$ , we obtain from (13), (17) and (18), the tip velocity in this phase:

$$v_{hd} = \frac{\gamma(1 - 2\gamma - \beta)}{1 - \gamma} , \quad (24)$$

and from this and (20), we have an expression for the density at site 2 and throughout the rest of the high density region:

$$\rho_+ = 1 - 2\gamma - \beta . \quad (25)$$

From (22), one can see that this phase is entered when:

$$\gamma = (\alpha - \beta)/(1 + \alpha) . \quad (26)$$

Due to the high density structure in the tip region we refer to the phase as the ‘*jammed*’ or *high density phase*. Note however that only on the phase boundary where  $v_s = v$ , is the shock and therefore the density profile stationary in the reference frame of the tip. In the rest of this phase  $v_s < v$ , and the shock moves away from the tip, resulting in an expanding high density region. Provided  $v_s > 0$ , the shock will also be moving away from the right boundary and the expanding high density region will never occupy the whole system. Using conditions (18) and (23), the condition  $v_s > 0$  becomes:

$$\frac{\alpha - \beta}{1 + \alpha} > \gamma > \frac{\alpha - \beta}{2} . \quad (27)$$

In order to fulfil our criterion for a steady state (stationary densities in our frame of reference as  $t \rightarrow \infty$ ) we should be in the reference frame of the shock. Then the density in front of the shock is given by  $1 - 2\gamma - \beta$  and the density behind is given by  $\alpha$ .

On the other hand if  $v_s < 0$ , then the shock moves backwards through the system until it reaches the right boundary. In this region a high density is maintained throughout the length of the lattice except for a boundary region next to the right boundary. The system may be considered to be in a high density steady state with the reference frame being the stationary frame where the right hand boundary is fixed. The condition  $v_s < 0$  becomes

$$\gamma < \frac{\alpha - \beta}{2} . \quad (28)$$

*Maximal current phase:* Both the high and low density phases are bounded by the condition that the roots  $\rho_{\pm}$  of (15) are real. Clearly, the roots (18) are real provided  $(1 - v)^2 > 4J$ , which implies using (13), that  $v < v_{max}$ , where the maximum velocity satisfies

$$v_{max} = \frac{2\beta + 3\gamma - 2\sqrt{\beta^2 + 3\gamma\beta + 2\gamma^2}}{\gamma} . \quad (29)$$

and the corresponding maximum current is  $J_{max} = (1 + \beta/\gamma)v_{max}$ .

When  $J = J_{max}$ , we have a single root of (15) and from (18) we deduce that the bulk density is

$$\rho_{max} = \frac{1 - v_{max}}{2}. \quad (30)$$

We refer to this phase as the maximal current phase; the flow is no longer controlled by the boundary condition  $\alpha$  rather it has saturated at a maximal flow rate,  $J_{max}$ . Note that  $\rho_{max} < 1/2$  and  $J_{max} < 1/4$ .

On a finite system of size  $N$ , in order to fix the boundary conditions, one takes  $J = J_{max} + O(1/N^2)$  [12, 2]. The iterative solution of (15) then yields a density profile decaying smoothly between both boundaries with an algebraic rather than an exponential decay of the density from the boundaries. Note that there is thus no natural reference frame in which we may define a steady state. Rather, the density at each site evolves as the system grows and we characterize this phase as quasi-stationary. We find the phase boundaries by considering the transitions to the maximal current phase from the low density phase, and from the high density phase:  $J_{ld} = J_{max}$  when

$$\gamma = \frac{\beta - 2\alpha\beta}{\alpha^2 - 1 + 2\alpha}, \quad (31)$$

and  $J_{hd} = J_{max}$  when

$$\beta = \frac{4\gamma - 2\gamma^2 - 1}{\gamma - 2}. \quad (32)$$

*3D Phase diagram:* In order to visualise the phase structure of the DEEP, we may construct a 3-dimensional phase diagram from the results of the simple mean-field theory. Figure 6 is a schematic representation of the three phase regions, joined by the phase boundary surfaces described above. On the diagram, one can see that in the limit of no growth ( $\gamma = 0$ ), the phase boundaries agree with those of the TASEP.

#### 4.1. The case $\beta = 0$

We may greatly simplify the equations of this model, by considering the case  $\beta = 0$ . This is the limit of no extraction from the tip and every particle reaching site 1 now contributes to the lattice growth. The current and velocity are therefore equal ( $J = v$ ). We now have in the steady state:

$$\rho_1 = v/\gamma \quad \rho_2 = \gamma v/(\gamma - v) \quad (33)$$

$$\rho_{i+1} = \frac{v(1 + \rho_i)}{1 - \rho_i} \quad i \geq 2. \quad (34)$$

The condition for the low density phase (22) reduces to  $\gamma > \alpha/(1 + \alpha)$  and the tip velocity is given by

$$v = J = \frac{\alpha(1 - \alpha)}{(1 + \alpha)}. \quad (35)$$

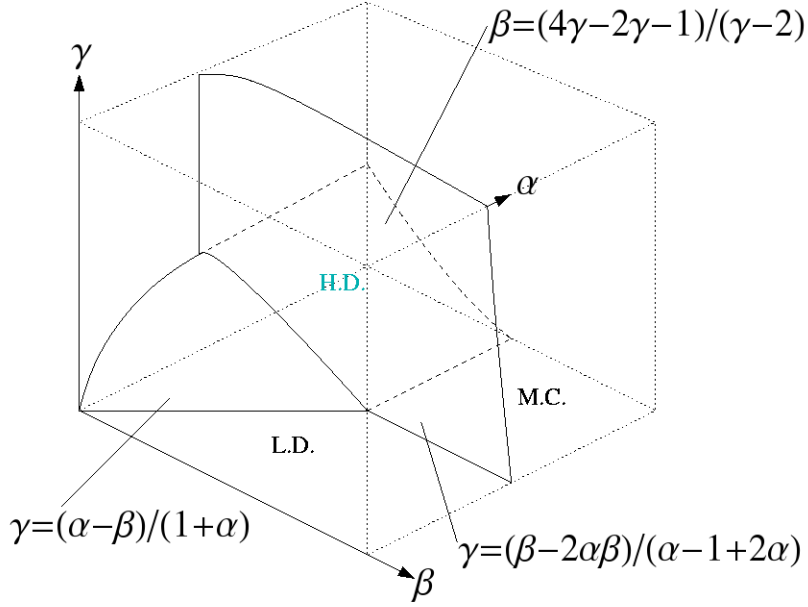


**Figure 6.** A schematic representation of the phase diagram in 3-D  $\alpha$ ,  $\beta$ ,  $\gamma$  parameter space for the simple mean-field approximation. The three phases are shown (without subregions). The  $\gamma = 0$  plane corresponds to the well known TASEP phase diagram.

Then, the condition that  $\rho_{\pm}$  be real becomes

$$J = v < 3 - 2\sqrt{2}, \quad (36)$$

which, with (35), implies

$$\alpha < \sqrt{2} - 1. \quad (37)$$

In the high density phase, where  $\gamma < \alpha/(1 + \alpha)$ , the tip velocity (24) is

$$v = J = \frac{\gamma(1 - 2\gamma)}{1 - \gamma}. \quad (38)$$

For  $\alpha/2 < \gamma < \alpha/(1 + \alpha)$  a dynamic shock exists in the system.

In the high density phase condition (36) together with (38) imply

$$\gamma < 1 - \frac{1}{\sqrt{2}}. \quad (39)$$

Therefore for the region bounded by  $\alpha > \sqrt{2} - 1$ ,  $\gamma > 1 - 1/\sqrt{2}$ , the system is in the maximal current phase, where the bulk density is  $\rho_{max} = \sqrt{2} - 1$  and the current is  $J_{max} = 3 - 2\sqrt{2}$ .

Monte-Carlo simulations of this system reveal that each of the predicted phases are indeed present. However, although the qualitative results of this simple mean-field theory appear to be correct, the predicted phase boundaries do not all agree with simulation (as we shall discuss in Section 7). Thus in order to more accurately predict the phase boundaries, we develop a refined mean-field theory.

## 5. Refined mean-field theory

In the approximation of the previous section, we ignored correlations between all pairs of sites in this system. In this section we introduce a refined mean field approximation which retains information about some correlations.

We might expect that sites 1 and 2 are in fact strongly correlated because when site 1 is vacated, so too is site 2. We can hope to improve our approximation by keeping the correlation  $\langle \tau_1 \tau_2 \rangle$  intact in (6-9) and beginning the iteration of (15) at site 3 instead of 2. Thus we approximate, for example,

$$\langle \tau_1 \tau_2 \tau_i \rangle = \langle \tau_1 \tau_2 \rangle \rho_i \quad i \geq 3. \quad (40)$$

To begin the recurrence we must find a new expression for  $\rho_3$  without factorising  $\langle \tau_1 \tau_2 \rangle$ , for example. Within the approximation, we have from (11),

$$\rho_3 = \frac{J + \gamma \langle \tau_1 \tau_2 \rangle}{1 - \langle \tau_2 \rangle}$$

and from (10)

$$\langle \tau_2 \rangle = J + \langle \tau_1 \tau_2 \rangle .$$

Combining these two relations gives

$$\langle \tau_1 \tau_2 \rangle = \frac{\rho_3 [1 - J] - J}{\gamma + \rho_3} . \quad (41)$$

Now we consider the steady state rates into and out of the configuration in which site 1 is vacant and site 2 is occupied:

$$\frac{d\langle \tau_2 [1 - \tau_1] \rangle}{dt} = 0 = \langle \tau_3 [1 - \tau_2] [1 - \tau_1] \rangle - \langle \tau_2 [1 - \tau_1] \rangle + \beta \langle \tau_1 \tau_2 \rangle . \quad (42)$$

We can identify the second term as the exact current from (10). Thus we obtain another exact expression for the steady state current:

$$J = \langle \tau_3 [1 - \tau_2] [1 - \tau_1] \rangle + \beta \langle \tau_1 \tau_2 \rangle . \quad (43)$$

Factorising beyond site 2, we may simplify and rearrange to give

$$\rho_3 = \frac{J - \beta \langle \tau_1 \tau_2 \rangle}{1 - J - \frac{J}{\gamma + \beta}} , \quad (44)$$

which along with (41), gives us a quadratic equation for  $\rho_3$

$$\rho_3^2 [1 - J - \frac{J}{\gamma + \beta}] + \rho_3 [(\gamma + \beta)(1 - J) - \frac{\gamma J}{\gamma + \beta} - J] - (\beta + \gamma)J = 0 . \quad (45)$$

This may be solved straightforwardly and used to deduce the three dimensional phase surfaces as in section 4.

### 5.1. The case $\beta = 0$

We consider again the simple case of  $\beta = 0$ . Then (44) reduces to

$$\rho_3 = \frac{J}{1 - J - \frac{J}{\gamma}} \quad (46)$$

The condition for a low density phase,  $\rho_3 < 1 - v - \alpha$ , is now

$$\alpha < \gamma \quad (47)$$

and the velocity as before is  $v = \alpha(1 - \alpha)/(1 + \alpha)$ . In the high density phase,  $\gamma < \alpha$  and the velocity is  $v = \gamma(1 - \gamma)/(1 + \gamma)$ . For  $\alpha/(2 - \alpha) < \gamma < \alpha$  a dynamic shock exists between the high density tip region  $\rho = \rho_+ = (1 - \gamma)/(1 + \gamma)$  and low density region  $\rho = \alpha$  far from the tip. The maximum current phase is attained when  $\alpha > \sqrt{2} - 1$  and  $\gamma > \sqrt{2} - 1$ .

### 5.2. Further correlations

We can repeat this mean-field improvement scheme by taking into account more correlations and correspondingly beginning the iteration of (15) further from the tip. One might expect that as further correlations are taken into account, the predicted phase diagram will converge toward the exact solution. As we shall see however, this is not always the case. We do not present the details of the further refined mean-field theory here as the equations become rather cumbersome, but the results for the phase boundaries are shown in Figure 7 and discussed later, in Section 7.

## 6. Symmetry and heuristic argument

An important feature which allows us to understand the phase behaviour of the TASEP (see Figure 2) is the presence of a symmetry between particles hopping in one direction and ‘holes’ hopping in the opposite direction. The high density particle phase can therefore be understood as a low density hole phase and vice versa.

Due to the moving boundary condition and the transition (3), there is no exact microscopic symmetry between particles and holes in the DEEP dynamics. However, it is true that particles leave/holes enter at the tip whereas particles enter/holes leave at the right end. It is plausible then that there exists some symmetry between the high density phase (low density of holes) and the low density phase (high density of holes). Indeed, the phase boundaries between the high, low and maximal current phases predicted by the refined mean-field theory in the limit of  $\beta = 0$  display a symmetry under the interchange  $\alpha \leftrightarrow \gamma$ . But while the the velocities in the two phases,  $\alpha(1 - \alpha)/(1 + \alpha)$  and  $\gamma(1 - \gamma)/(1 + \gamma)$ , are also symmetric under the interchange  $\alpha \leftrightarrow \gamma$ , the bulk densities in these phases,  $\alpha$  and  $(1 - \gamma)/(1 + \gamma)$ , are not symmetric.

In the case of  $\beta \neq 0$ , the refined mean-field approximation no longer displays a particle hole symmetry. A heuristic argument however, does lead to a 3D phase transition between the high and low density phases which maintains a symmetry between input rate  $\alpha$  and output rate  $\beta + \gamma$ .

If we ignore the density structure near the tip and assume that in the high density phase there exists a single high density value associated with the tip:  $\rho_1 = \rho_{bulk}$ , in the same way that in the low density phase, we have a single density  $\alpha$  associated with the input end of the lattice, then from (11-13) we have the following:

$$v = \gamma\rho_1 = \frac{\rho_1(1 - \rho_1)}{1 + \rho_1 + \frac{\beta}{\gamma}}. \quad (48)$$

This is solved to give the bulk density:

$$\rho_1 = \rho_{bulk} = \frac{1 - \gamma - \beta}{1 + \gamma}, \quad (49)$$

and associated high density velocity:

$$v = \frac{\gamma(1 - \gamma - \beta)}{1 + \gamma}. \quad (50)$$

As before we appeal to the concept of a shock discontinuity in the system. The low density phase is reached when the shock velocity  $(1 - \rho_+ - \alpha)$  is greater than the tip velocity (50), which corresponds to a phase transition at:

$$\alpha = \beta + \gamma, \quad (51)$$

suggesting an exact correspondence between the balancing of input and output rates and the transition between high and low density phases. This boundary is the same as that derived by the refined mean-field theory in the limit  $\beta = 0$  and is in fact very close to that derived in the case  $\beta \neq 0$  (see Figure 11 in the next Section). The remaining phase boundaries are derived as in section 4.

## 7. Phase Diagrams and Simulation

As we have seen, the mean-field theories discussed above predict the same phases but with differing phase boundaries. The transition between the low density and maximal current phases (31) is the same in each theory, however the transitions between other phases vary significantly. For comparison, the basic 2-D phase diagrams for the simple, refined and further refined mean-field theories in the limit of  $\beta = 0$  are plotted in Figure 7. Note in particular, a large difference in the boundary between subregions in the low density phase where the tip density decays from above or below  $\alpha$ . The high to low density transition is also significantly different in the simple mean-field theory. In order to explore the exact phase structure of the DEEP model, and identify which of the theories best describes the exact behaviour of the model, we turn now to a numerical discussion. For simplicity, we

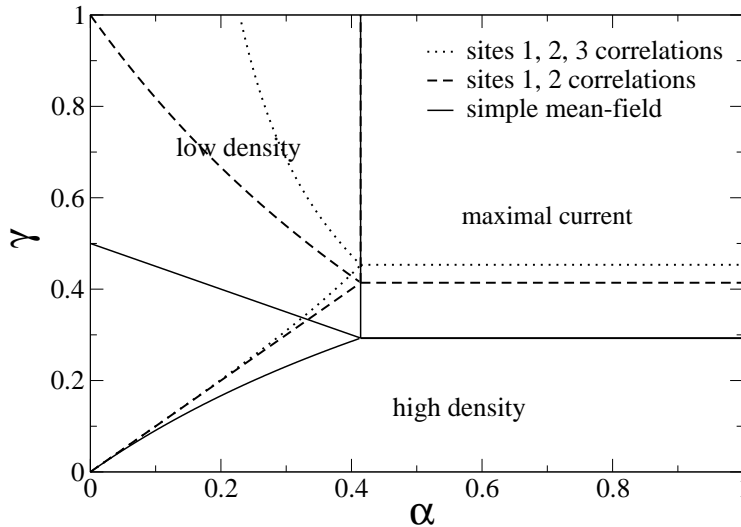


**Figure 7.** Comparison of three mean-field approximations in the case  $\beta = 0$ .

work primarily in the  $\beta = 0$  limit. Note that in this limit the refined mean-field theory of Section 5 and the heuristic argument of Section 6 are in agreement.

Monte-Carlo simulations of the DEEP were carried out across the parameter space. The simulated lattice comprises an array of binary values representing  $\tau_i$ . For each update, a site in the lattice is selected randomly and a transition is attempted with a probability defined by the rates (1-4). One time-step consists of  $N$  such updates, so that on average each site is updated once per time-step. Thus as  $N$  increases, so does the number of updates per time step, in order to keep our time unit constant. Note that during one time-step the system may increase in length. In principle, this would affect our unit of time, however, such an increase, typically of one lattice unit, will be insignificant in the large  $N$  limit.

Our aim is to allow the system to reach a steady state, and then we may calculate quantities such as site densities, particle flux and rate of change in lattice length. A problem with this method is that as the system grows,  $N \rightarrow \infty$  and the computational cost for each time-step increases. We may however minimise this problem by considering only a fixed length portion of the lattice in a particular frame of reference. For example, in the low density phase we expect that the density tends exponentially to  $\alpha$ , so we may truncate the lattice at site  $M < N$  and simulate only the  $M$  sites nearest the tip. This method will only work for the steady state phases which are clearly defined in some reference frame. For the maximal current phase and shock region, we still consider the whole system.

An example of each type of density profile is plotted in Figure 8. In the low density phase, the steady state densities are calculated by averaging the occupancy over many time-steps in the reference frame of the tip. On the other hand, in the high density phase, the steady states are defined in the reference frame of the input and the average occupancies

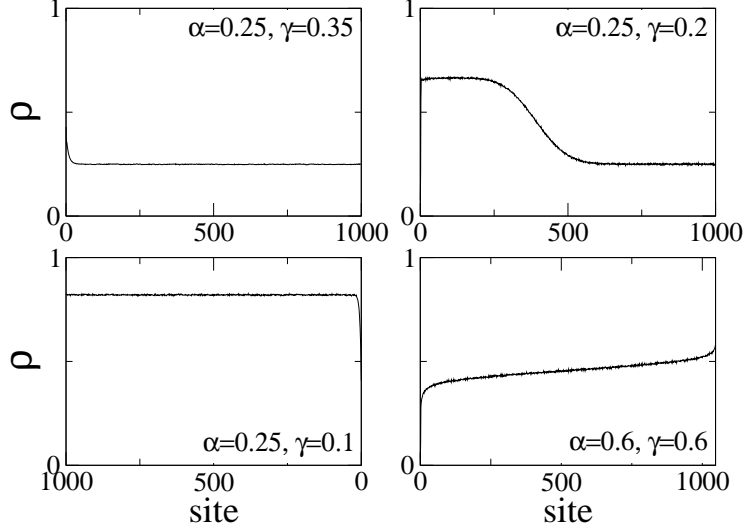


**Figure 8.** Density profiles from the different phases of the dynamically extending exclusion process. From top left: Low density, shock profile, high density and maximal current phase. Note that since the high density profile is calculated in the reference frame of the input, the sites are labelled from right to left, site 0 being where particles are injected.

are calculated from this frame. For profiles in the shock region and the maximal current phase, the system is never in a truly stationary state, and to view the density profile, we must find the average occupancies at a fixed length and thus fixed time. The densities here are calculated by averaging over many arrays which have grown to a specified length.

One property which may be used to locate the exact positions of the phase transitions is the lattice tip velocity, which is given by a simple function of the parameters and changes form across the phase boundaries (see equations (21,24,29)). We find from the velocity of the simulated lattices, that the first refined mean-field theory appears to predict the correct form for the tip velocity and the correct phase transitions. Figure 9 shows the velocity of a simulated lattice plotted for different values of  $\gamma$ , against the refined mean-field expression for the velocity. The velocities closely follow the predicted curve (35) and as expected, a phase transition takes place at  $\alpha = \gamma$ , where the velocity becomes independent of  $\alpha$ . The maximum velocity is reached when  $\alpha = \sqrt{2} - 1$  and  $\gamma \geq \sqrt{2} - 1$ .

Further evidence in support of the refined mean-field theory can be found by exploring the density profiles of the low density region, where the three theories predict different transitions between profiles which decay at the tip from below and above  $\alpha$ . In Figure 10, we see that the transition appears to agree with that predicted by the first refined theory, while being at odds with both the further refined and the simple approximations.

For completeness, we consider now the case of non zero  $\beta$ . In Figure 11 the simulated growth velocities are compared to the refined mean-field theory velocity functions for the high and low density phases for  $\beta \neq 0$ . The high density velocity obtained from the heuristic



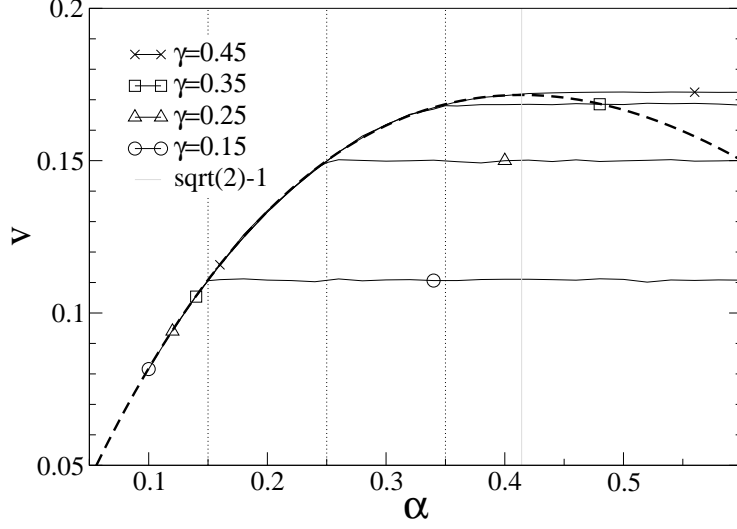


**Figure 9.** The tip velocity plotted against  $\alpha$  for  $\gamma = 0.15..0.45$  and  $\beta = 0$ . For  $\gamma < \sqrt{2} - 1$ , a clear phase transition occurs when  $\alpha \approx \gamma$ . This transition is from the *low density phase* where  $v = \frac{\alpha(1-\alpha)}{1+\alpha}$  to the *high density phase*, where the velocity is  $\alpha$  independent. For clarity, dotted lines are used to indicate  $\alpha = \gamma$ . When  $\gamma = 0.45 > \sqrt{2} - 1$ , the maximum velocity occurs as predicted at  $\alpha = \sqrt{2} - 1$ .

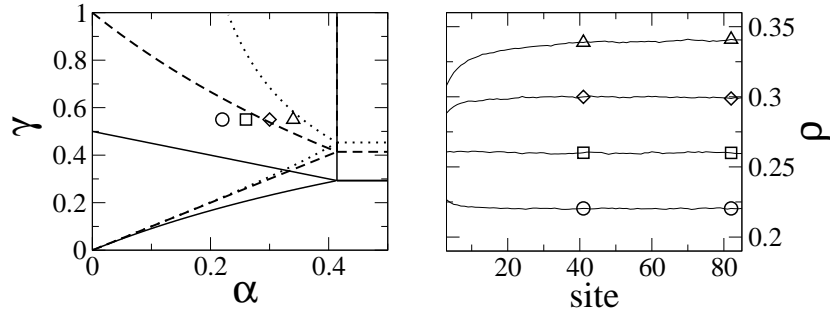


**Figure 10.** In the left-hand plot, the simple (solid line), refined (dashed line) and further refined (dotted line) phase boundaries are shown. Simulations were carried out in the low density phase, across the predicted boundary between profiles with a decay from above and below  $\alpha$  (parameter values indicated with symbols). The resulting profiles, shown in the right-hand plot, display a transition that is in best agreement with the refined mean-field transition line.

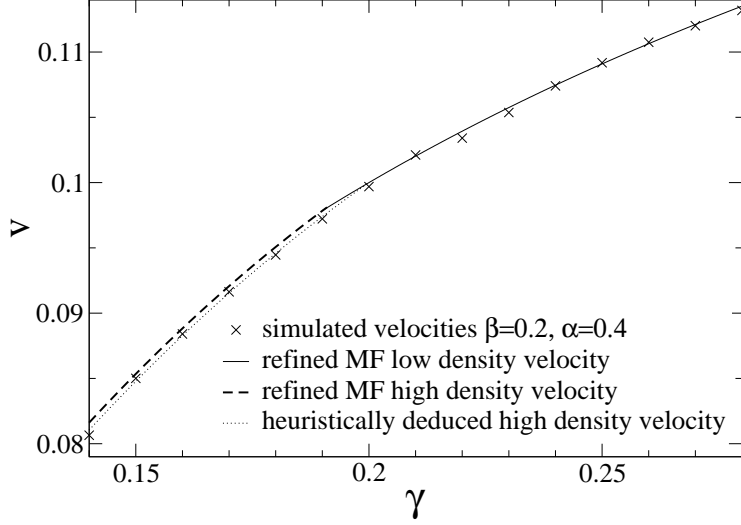


**Figure 11.** Theoretical and simulation results for the tip velocity as a function of  $\gamma$ , given for fixed values of  $\alpha$  and  $\beta > 0$ . The data points show simulation results, fitted to the heuristic and refined mean-field functions for the tip velocity in the high and low density phases. The low density velocity is the same for heuristic and mean-field approaches and is given by (21). The high density velocity function is found in the refined mean-field theory by solving equation (45) and inequality  $\rho_3 < 1 - v - \alpha$  (explicit expression for the high density velocity is not presented here). The heuristic high density velocity is given by (50). The phase transition occurs at approximately  $v_{ld} = v_{hd}$

argument is also shown and one may see that this coincides rather closely with the refined mean-field result. Due to the nature of Equations 45 and inequality  $\rho_3 < 1 - v - \alpha$  which must be solved simultaneously, in this case it is simpler to work with the velocity as a function of  $\gamma$ . Therefore, simulations were carried out with fixed values  $\alpha = 0.4$  and  $\beta = 0.2$ , in the range close to the phase transition  $\gamma = 0.14..0.28$ . We see a good agreement of the simulation data points with the high density and the low density velocity functions predicted by the refined mean field theory. Note however, that in the high density phase the simulation results appear after all to be in best agreement with the heuristic result for the velocity (50). The phase transition occurs as expected where the high and low velocity functions meet.

Finally, we present the detailed 2-D phase diagram of the first refined mean-field theory in the limit  $\beta = 0$ , shown in Figure 12. The diagram is split into the three distinct phases: high, low and maximal current. The low density phase is split into two subregions I and II, where the tip decays to the bulk density from above and below respectively. The shock region, where the shock recedes from both boundaries, is indicated within the high density phase. We believe this to be at least an accurate approximation to the exact phase structure as we discuss in the next section.

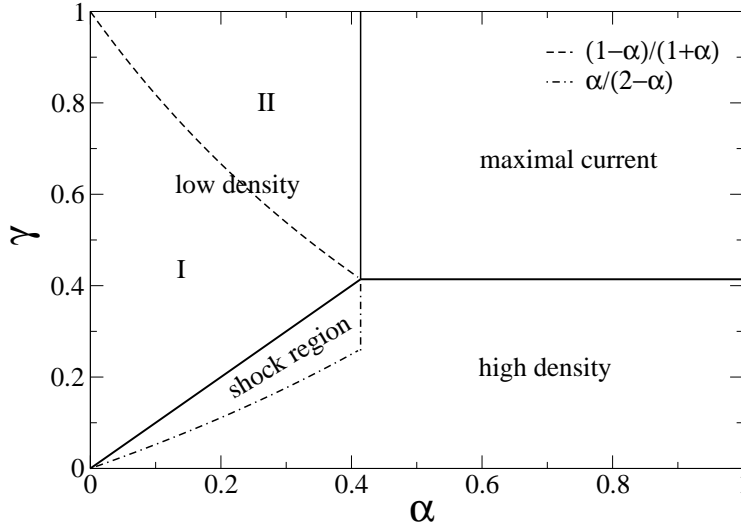


**Figure 12.** The phase diagram obtained from the refined mean-field approximation in the limit  $\beta = 0$ . Three phases are shown. The low density phase is split into subregions I and II, indicating regions where the density profile decays from above and below the bulk density respectively. The shock region is indicated within the high density phase.

## 8. Conclusion

In this work we have studied a generalisation of the open boundary TASEP to a dynamically extending lattice and characterised a generalised phase diagram in the  $\alpha, \beta, \gamma$  parameter space. The model provides an example of a system where the dynamics of the microscopic constituents couple to and determine the dynamics of the containing structure. We conclude that steady states can exist in this system, where the lattice is continuously extending from one end while being supplied with particles from the other end.

The well-known phases of the open boundary TASEP are reflected in the phase diagram of this model (Figure 12). The low density phase has structure in the density profile near the tip and the bulk density is controlled by the low input rate at the opposite boundary. In the high density phase the bulk density is controlled by the tip dynamics and there is structure in the density profile near the opposite boundary. In between we have a shock region where a high density and a low density region are separated by a moving shock which in fact recedes from both boundaries. The shock region of the phase diagram extends the known phases and adds to the variety of shock formation phenomena which have been observed in the TASEP and related models[15, 16, 17, 18]. Finally, the maximal current phase is present but with bulk density  $< 1/2$ . However, in this model the maximal current phase is not strictly a steady state as the current and the density profile continue to evolve as the system grows.

We have used several mean-field approximations and find that while the simplest

mean-field approach successfully predicts the qualitative behaviour of the phases, the phase boundaries are not accurately predicted. However, a refined mean-field approximation which takes into account the correlation between sites one and two predicts a phase diagram which appears to coincide very closely with simulation results and is very close to that deduced by the heuristic argument of Section 6. It would be of interest to know whether in fact the predictions, summarised for the  $\beta = 0$  case in Figure 12, could be exact. Interestingly, taking into account a further correlation appeared to worsen the predicted phase diagram. This sort of negative result has been encountered in mean-field approximation schemes in the past [19]. For example it was found in the ZGB surface reaction model that a pair mean-field approximation successfully locates a discontinuous phase transition, while a four-site approximation seems to do worse [20].

The DEEP was initially formulated as a model derived from the TASEP of a biophysical growth process, namely fungal hyphal growth [9] and provides a simple framework which may find application in a broader context. The TASEP has been successfully developed to describe various biophysical transport problems by incorporating additional biological detail such as dynamic instabilities and heterogeneity [21, 22, 23, 24, 25]. It could prove fruitful to study the effects of such features in the present model.

## Acknowledgments

We would like to thank Wilson Poon, Nick Read and Graham Wright for their encouragement and discussions on fungal biology, and Graeme Ackland for helpful comments. KEPS thanks the EPSRC for funding.

## References

- [1] D. Mukamel, pp237–258 in *Soft and Fragile Matter: Nonequilibrium Dynamics, Metastability and Flow*, Eds M. E. Cates and M. R. Evans, IoP Bristol 2000
- [2] R. A. Blythe and M. R. Evans arXiv:0706.1678
- [3] D. Chowdhury, A. Schadschneider and K. Nishinari *Phys. Life Revs.* **2**, (2005), 318
- [4] Y. Aghababaie, G. I. Menon and M. Plischke *Phys. Rev. E* **59**, (1999), 2578
- [5] R Lipowsky, S Klumpp and Th M. Nieuwenhuizen *Phys. Rev. Lett.* **87**, (2001), 10810
- [6] S Klumpp and R Lipowsky *J. Stat. Phys.* **113**, (2003), 233
- [7] E. Frey, A. Parmeggiani, and T. Franosch, Collective Phenomena in Intracellular Processes, *Genome Informatics* **15**, (2004), 46
- [8] C. T. MacDonald, J. H. Gibbs and A. C. Pipkin, *Biopolymers*, **6**, (1968), 1
- [9] K. E. P. Sugden, M. R. Evans, W. C. K. Poon and N. D. Read *Phys. Rev. E* **75**, 031909 (2007)
- [10] M. R. Evans and K. E. P. Sugden, *Physica A*, (2007), doi:10.1016/j.physa.2007.04.078
- [11] S. A. Nowak, P. W. Fok, and T. Chou *Phys. Rev. E* **76**, 031135 (2007)
- [12] B. Derrida, E. Domany and D. Mukamel *J. Stat. Phys.* **69**, (1992), 667
- [13] B. Derrida, M. R. Evans, V. Hakim and V. Pasquier *J. Phys. A*, **26**, (1993), 1493
- [14] G. Schütz and E. Domany, *J. Stat. Phys.*, **72**, (1993), 277

- [15] A. Parmeggiani, T. Franosch and E. Frey *Phys. Rev. Lett* **90**, (2003), 086601
- [16] M. R. Evans, R. Juhász and L. Santen, *Phys. Rev. E* **68**, (2003), 026117
- [17] V. Popkov, A. Rakos, R.D. Willmann, A.B. Kolomeisky, G.M. Schutz *Phys. Rev. E*, **67**, (2003), 066117
- [18] S. Mukherji and S. M. Bhattacharjee *J. Phys. A, J. Phys. A Letters*, **38**, (2005), L285
- [19] D. ben Avraham and J. Kohler *Phys. Rev. A*, **45**, (1992), 8358
- [20] R. Dickman *private communication*
- [21] M. Dogterom, and S. Leibler *Phys. Rev. Lett.*, **70**, 1347, 1993
- [22] T. Antal, P. L. Krapivsky and S. Redner *J.Stat.*, (2007), L05004
- [23] M R Evans, T Hanney and Y Kafri *Phys. Rev. E* **70**, (2004), 066124
- [24] G. A. Klein, K. Kruse, G. Cuniberti and F. Jülicher *Phys. Rev. Lett.* **94**, (2005), 108102
- [25] O. Campas, Y Kafri, K B Zeldovich, J Casademunt, J-F Joanny *Phys. Rev. Lett.* **97**, (2006), 0381012